Dalton Transactions

PAPER

View Article Online
View Journal | View Issue



Cite this: *Dalton Trans.*, 2014, **43**, 4854

# The quenching of fluorescence as an indicator of donor-strength in *meso* arylethynyl BODIPYs†

Rajneesh Misra,* Bhausaheb Dhokale, Thaksen Jadhav and Shaikh M. Mobin

Received 29th October 2013,
Accepted 18th December 2013

DOI: 10.1039/c3dt53056f

www.rsc.org/dalton

A series of *meso* arylethynyl BODIPYs (**2a–2h**) were designed and synthesized by the Pd-catalyzed Sonogashira cross-coupling reaction. The effects of the donor on the photophysical properties of the BODIPYs were explored. The DFT optimized structures and crystal structures show the planar orientation of the donor group with respect to the acceptor BODIPY, which favors a high degree of conjugation and induces strong donor–acceptor interactions. The quenching of fluorescence was correlated with the electron donating strength of the donor. The anthracene, pyrene and triphenylamine were found to have a stronger electron donating ability than the *p*-methoxyphenyl, phenanthrene, 1-naphthalene, biphenyl, and 2-naphthalene moieties. This was further supported by computational calculations and electrochemical analysis. The single crystal structures of BODIPYs **2d** and **2e** are reported, which show marvellous supramolecular structures.

## Introduction

In recent years BODIPY chemistry has gained momentum, which is reflected from their share in most of the journals.[1] BODIPY dyes distinguish themselves from others due to strong absorption, sharp fluorescence and high thermal stability.[2] These properties of the BODIPYs make them a potential candidate in organic electronics and photonics.[3] Our group is interested in the design of donor–acceptor molecular systems for photonic applications.[4] The BODIPY unit acts as strong acceptor. Therefore the functionalisation of BODIPY dyes with donors will result in donor–acceptor (D–A) type molecular systems.[5] Various strategies are reported in the literature for the functionalisation of the BODIPY dyes at the *meso* position as well as the pyrrolic positions.[6] In *meso* aryl functionalized BODIPY, the *meso* substituent adopts an orthogonal orientation with respect to the BODIPY core, which hinders the electronic communication. One can overcome this problem by introducing the ethynyl linkage at the *meso* position, so that the substituent and the BODIPY will be planar, with respect to each other for a better electronic communication. Wim Dehaen has introduced an efficient synthetic strategy for the incorporation of the ethynyl linkage at the *meso* position.[7]

Our previous report on ferrocenyl BODIPYs has established that the *meso* alkynylated BODIPYs show superior electronic communication than the pyrrolic alkynylated BODIPYs.[8] This encouraged us to study the effect of various donors at the *meso* position of the BODIPY *via* an ethynyl linkage. In this report we have incorporated various donors at the *meso* position of the BODIPY *via* an ethynyl linkage and studied their structural, electronic, photophysical, and electrochemical properties.

## Results and discussion

The *meso*-arylethynyl BODIPYs **2a–2h** were synthesized by the palladium catalyzed Sonogashira cross-coupling reaction of 8-chloro BODIPY **1** with respective arylethynes (**a–h**) as shown in Scheme 1. The 8-chloro BODIPY **1**, was synthesized from dipyrrylketone.[7] The dipyrrylketone was reacted with $POCl_3$ followed by *in situ* deprotonation by base and complexation with $BF_3$ etherate, which resulted 8-chloro BODIPY **1** in a 59% yield. The dipyrrylketone was synthesized by the condensation reaction of thiophosgene and pyrrole, followed by oxidation with $H_2O_2$ under basic condition.[9] The arylethynes **a–h** were synthesized from reported procedures.[10]

The Pd-catalyzed Sonogashira cross-coupling reaction of 8-chloro BODIPY **1**, with the respective arylethynes at 0 °C resulted BODIPYs **2a–2h** in 44 to 77% yields. These reactions were completed within half an hour due to the high reactivity of 8-chloro BODIPY. The BODIPYs **2a–2h** were well characterized by $^1$H NMR, $^{13}$C NMR and HRMS techniques. The

*Department of Chemistry, Indian Institute of Technology Indore, Indore 452 017, India. E-mail: rajneeshmisra@iiti.ac.in*

†Electronic supplementary information (ESI) available: general experimental methods, and copies of $^1$H, $^{13}$C NMR, and HRMS spectra of all new compounds, crystallographic information files (CIFs) for compounds **2d** and **2e**, the thermal and photophysical properties, the electrochemical properties, and the theoretical calculations. CCDC number 967406 for **2d** and 967407 for **3e**. For ESI and crystallographic data in CIF or other electronic format see DOI: 10.1039/c3dt53056f

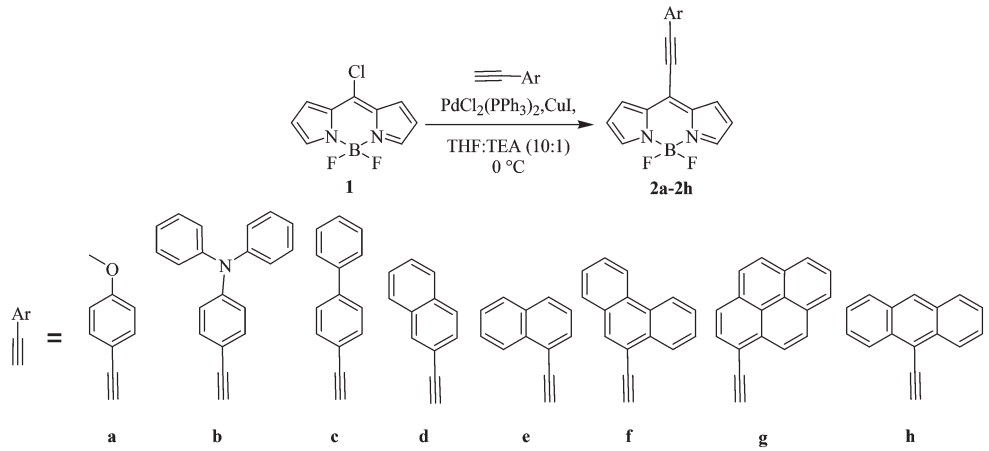


**Scheme 1** The synthesis of *meso*-arylethynyl BODIPYs **2a–2h**.

BODIPYs **2d** and **2e** were also characterized by the single crystal X-ray diffraction technique.

The typical $^1$H NMR spectrum of the BODIPY derivatives show two α pyrrolic protons as a singlet at ~7.8 ppm, whereas the β and β′ protons appear as doublets at ~6.6 and ~7.7 ppm. The protons of the aryl substituent appear in the aromatic region.

The thermal stability is one of the key criteria for optoelectronic applications. The thermal properties of the *meso*-arylethynyl BODIPYs (**2a–2h**) were investigated using thermogravimetric analysis (TGA) by heating the BODIPYs in a nitrogen atmosphere at the heating rate of 10 °C per minute and monitoring the weight loss against temperature (Fig. 1). The TGA analysis shows that the *meso*-arylethynyl BODIPYs were stable enough up to 350 °C. The decomposition temperature at 10% weight loss is shown in Table 1, indicating the good thermal stability of the BODIPYs.

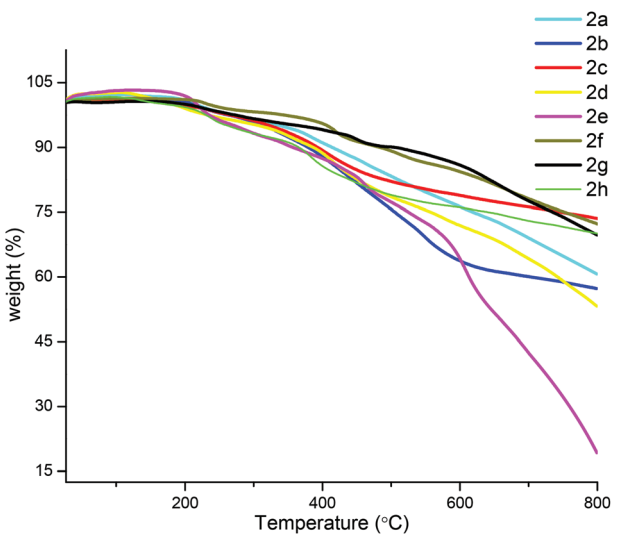


**Fig. 1** The TGA plot of the *meso*-arylethynyl BODIPYs **2a–2h**.

**Table 1** Photophysical and thermal properties of *meso*-arylethynyl BODIPYs **2a–2h**

| BODIPY | $\lambda_{S0\rightarrow S1}$ (nm) | $\varepsilon \times 10^4$ ($M^{-1}$ $cm^{-1}$)[a] | $\lambda_{em}$[b] (nm) | Stokes shift ($cm^{-1}$) | $\Phi_F$[c] | $T_d$[d] (°C) |
|---|---|---|---|---|---|---|
| **2a** | 538 | 4.4 | 552 | 472 | 0.23 | 414 |
| **2b** | 540 | 5.0 | —[e] | —[e] | —[e] | 379 |
| **2c** | 543 | 3.8 | 558 | 495 | 0.18 | 392 |
| **2d** | 544 | 4.9 | 559 | 493 | 0.19 | 386 |
| **2e** | 545 | 3.5 | 561 | 523 | 0.19 | 357 |
| **2f** | 546 | 4.4 | 563 | 554 | 0.20 | 484 |
| **2g** | 548 | 4.5 | —[e] | —[e] | —[e] | 504 |
| **2h** | 553 | 4.6 | 565 | 384 | 0.02 | 365 |

[a] Recorded at $S_0\rightarrow S_1$. [b] Excited at $\lambda_{S0\rightarrow S1}$. [c] Determined using Rhodamine 6G as the standard ($\Phi$ = 0.88, in ethanol). [d] The decomposition temperature at 10% weight loss, determined by TGA. [e] The BODIPYs are non emissive.

## Photophysical properties

The photograph of the BODIPYs **2a–2h** in a dichloromethane solvent in day light and in UV light is displayed in Fig. 2. The coloring pattern of the BODIPYs reflects the D–A interaction. The BODIPYs **2b**, **2g** and **2h** are non-fluorescent with a dark purple color indicating a strong D–A interaction, whereas the BODIPYs **2a** and **2c–2f** are fluorescent with a yellow–red shade which indicates a moderate D–A interaction.

The UV-vis absorption spectra of the *meso*-arylethynyl BODIPYs **2a–2h** were recorded in dichloromethane (Fig. 3), and the corresponding data are shown in Table 1. The BODIPYs **2a–2h** show a strong absorption band between 538 and 553 nm which corresponds to the $S_0\rightarrow S_1$ transition with a high extinction coefficient, and a shoulder at a higher energy region corresponding to the respective vibronic transition of the BODIPY. The BODIPYs **2a–2h** show a red shift of 35–50 nm in the $S_0\rightarrow S_1$ absorption band compared to 8-chloro BODIPY **1** (Table 1) due to enhanced conjugation. The red shift in the $S_0\rightarrow S_1$ absorption band follows the order of **2h** > **2g** > **2f** > **2e** > **2d** > **2c** > **2b** > **2a**. The BODIPY **2b** shows a shoulder in the

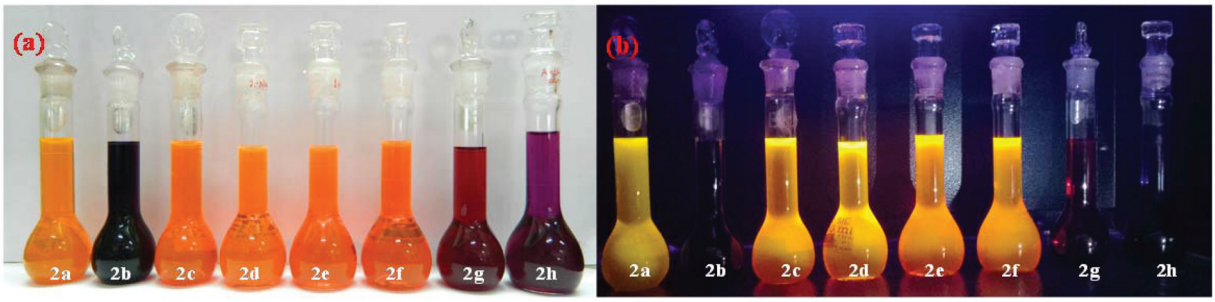


Fig. 2 The BODIPYs **2a–2h** in dichloromethane at a concentration of $10^{-4}$ M (a) in day light and (b) in UV light.

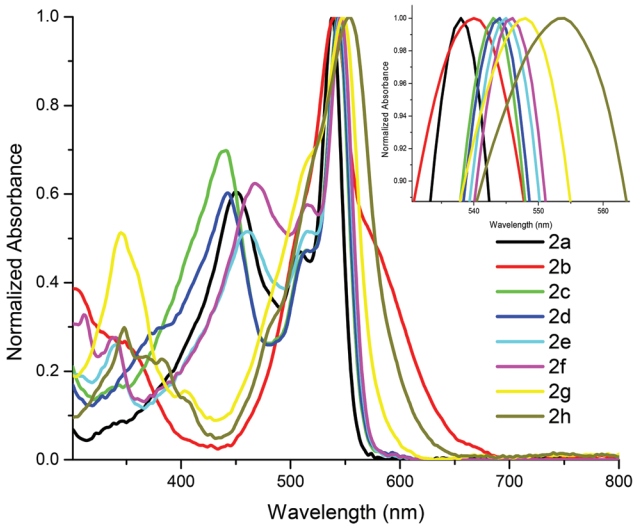


Fig. 3 The normalized UV-vis absorption spectra of the *meso*-arylethynyl BODIPYs **2a–2h** recorded in dichloromethane, the inset shows the enlarged view.

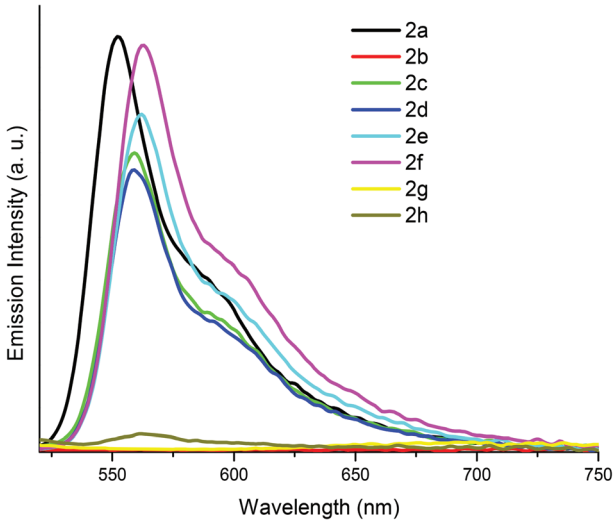


Fig. 4 The emission spectra of the *meso*-arylethynyl BODIPYs **2a–2h**, recorded in dichloromethane.

$S_0 \rightarrow S_1$ absorption band at a low energy region, which can be attributed to a charge transfer.[11]

The emission properties of the *meso*-arylethynyl BODIPYs **2a–2h** were studied in dichloromethane (Fig. 4) and the corresponding data are given in Table 1. The *meso*-arylethynyl BODIPYs **2a**, **2c–2f** and **2h** emit in the 520–650 nm region with a Stokes shift ranging from 380–550 $cm^{-1}$. The fluorescence quantum yields of the BODIPYs **2a–2h** were decreased drastically compared to 8-chloro BODIPY **1**. The BODIPYs **2a** and **2g** were non-emissive in nature. The quenching of the fluorescence is may be due to the intramolecular energy transfer from the aryl moiety to the BODIPY.[12] The trend in the quenching of the fluorescence can be correlated to the electron donating ability of the aryl substituent. In addition the electron donating ability lesser will be the quantum yield. From the quantum yield values the electron donating ability of the aryl substituent follows the order: **2b** > **2g** > **2h** > **2d** > **2c** > **2e** > **2f** > **2a**.

## Electrochemical properties

The electrochemical properties of the *meso*-arylethynyl BODIPYs were investigated by the cyclic voltammetric and differential pulse voltammetric (CV and DPV) techniques (Fig. 5). The potentials were referenced against $Fc/Fc^+$ as per IUPAC guidelines.[13] The redox peaks were mostly irreversible or quasi reversible. The BODIPYs **2a–2h** show two oxidation and two reduction waves corresponding to the formation of a dication and dianion radical, respectively. The stronger the D–A interaction, the better the delocalization of the electrons from the donor aryl moiety to the acceptor BODIPY moiety, showing the easier oxidation and more difficult reduction of the BODIPYs.

The BODIPY **2b** shows the easiest oxidation and the hardest reduction indicating the pronounced delocalization of the electron density of the donor triphenylamine moiety on the acceptor BODIPY; on the other hand, the BODIPY **2c** shows easiest reduction and the hardest oxidation indicating the poor delocalization of the electrons of the donor aryl on the acceptor BODIPY. The other BODIPYs show redox peaks at intermediate potentials. The redox properties suggest a strong D–A interaction in the BODIPYs **2b**, **2g** and **2h** and moderate D–A interactions in **2a** and **2c–2f** (Table 2).

## Theoretical calculations

The electronic distribution of the *meso*-arylethynyl BODIPYs could be better understood by DFT calculations. The energy

 

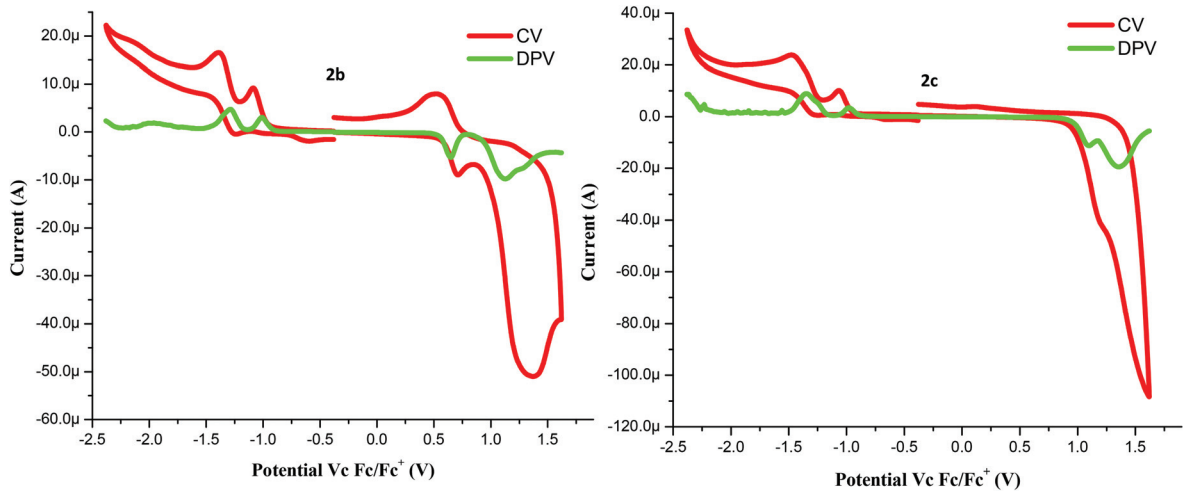


Fig. 5 The overlayed CV and DPV plots of the *meso*-arylethynyl BODIPYs **2b** and **2c**.

Table 2 The electrochemical properties of the *meso*-arylethynyl BODIPYs **2a–2h**[a]

| BODIPY | $E^2$ oxid[b] | $E^1$ oxid[b] | $E^1$ red[b] | $E^2$ red[b] |
|---|---|---|---|---|
| **2a** | 1.28 | 1.07 | −1 | −1.35 |
| **2b** | 1.13 | 0.65 (broad) | −1.01 | −1.29 |
| **2c** | 1.35 | 1.1 | −0.98 | −1.35 |
| **2d** | 1.28 | 1.07 | −0.99 | −1.28 |
| **2e** | 1.28 | 1.07 | −1.01 | −1.37 |
| **2f** | 1.32 | 0.99 | −1.01 | −1.32 |
| **2g** | 1.22 (broad) | 0.85 | −1 | −1.37 |
| **2h** | 1.16 (broad) | 0.89 | −1 | −1.4 |

[a] The electrochemical analysis was performed in a 0.1 M solution of $Bu_4NPF_6$ in dichloromethane at a 100 mV $s^{-1}$ scan rate, *versus* $Fc/Fc^+$. [b] Irreversible wave.

minimized structures show the planar orientation of the BODIPY core with respect to the *meso* aryl substituent, which indicates a better electronic communication. The energy optimized structures closely resemble the single crystal X-ray structures. The frontier molecular orbital plots are displayed in Fig. 6. The LUMO in the *meso*-arylethynyl BODIPYs **2b**, **2g** and **2h** is majorly contributed by the BODIPY moiety, and the HOMO is contributed by the arylethynyl moiety, supporting strong D–A interactions. In the *meso*-arylethynyl BODIPYs **2a**, **2c–2f** the HOMO is localized on the BODIPY unit and the LUMO is distributed on the whole molecule but majorly on the arylethynyl unit suggesting moderate D–A interactions.

### Single crystal X-ray diffraction studies

The single crystals of the BODIPYs **2d** and **2e** were obtained by the slow evaporation of a mixture of chloroform and hexane solution (1 : 3 ratio). The BODIPYs **2d** and **2e** crystallize in the space groups $P2_12_12_1$ and $P2/c$, respectively. The crystal structure and data refinement parameters and the distances and angles of the intermolecular interactions in the crystal structures are summarized in Tables S1 and S3, respectively (ESI†).

The crystal structure of the BODIPYs **2d** and **2e** are shown in Fig. 7. The torsional angle between the BODIPY and aryl moiety are shown in Table S2 (ESI†). The crystal structures show the highly planar orientation of the aryl moiety and BODIPY unit.

In the packing of BODIPY **2d**, the π–π staking interaction between the two BODIPY units forms a staircase like structure. Such a staircase like structure connects another stair case like structure in a perpendicular direction *via* a C(17)–H(17)···π (pyrrolic) interaction. If flipped to view along the *a*-axis it looks L-shaped, hiding behind the π-staked molecules. The L-shaped structure further grows to form a complex 3-D structural motif (Fig. 8 and Fig. S3 (ESI†)).

Similarly in the crystal structure of **2e** two molecules connect to each other in a head to tail fashion *via* another molecule by two mutual F(1)···H(9)–C(9) and a F(2)···H(18)–C(18) interaction forming a 2D chain. Two such chains connect to another chain in an anti-parallel fashion by face to face π···π staking interactions between two BODIPY units (Fig. 9a), these chains further cross link to other chains forming a complex 3D packing diagram along the tilted *c*-axis. In the packing diagram the molecules orient in such a way that the aryl part of the BODIPY units is at the centre and surrounded by the BODIPY moiety (Fig. 9b).

## Conclusion

In summary, we have reported the synthesis of *meso*-arylethynyl BODIPYs. The photophysical and electrochemical properties of the BODIPYs can be tuned by varying the strength of the donor. The DFT calculations and photophysical and electrochemical properties suggest strong donor–acceptor interactions in the BODIPYs **2b**, **2g** and **2h**, and moderate interactions in **2a**, and **2c–2f**. The quenching of fluorescence can be used as a measure of the relative electron donating strength of the aryl substituent. The crystal structures show

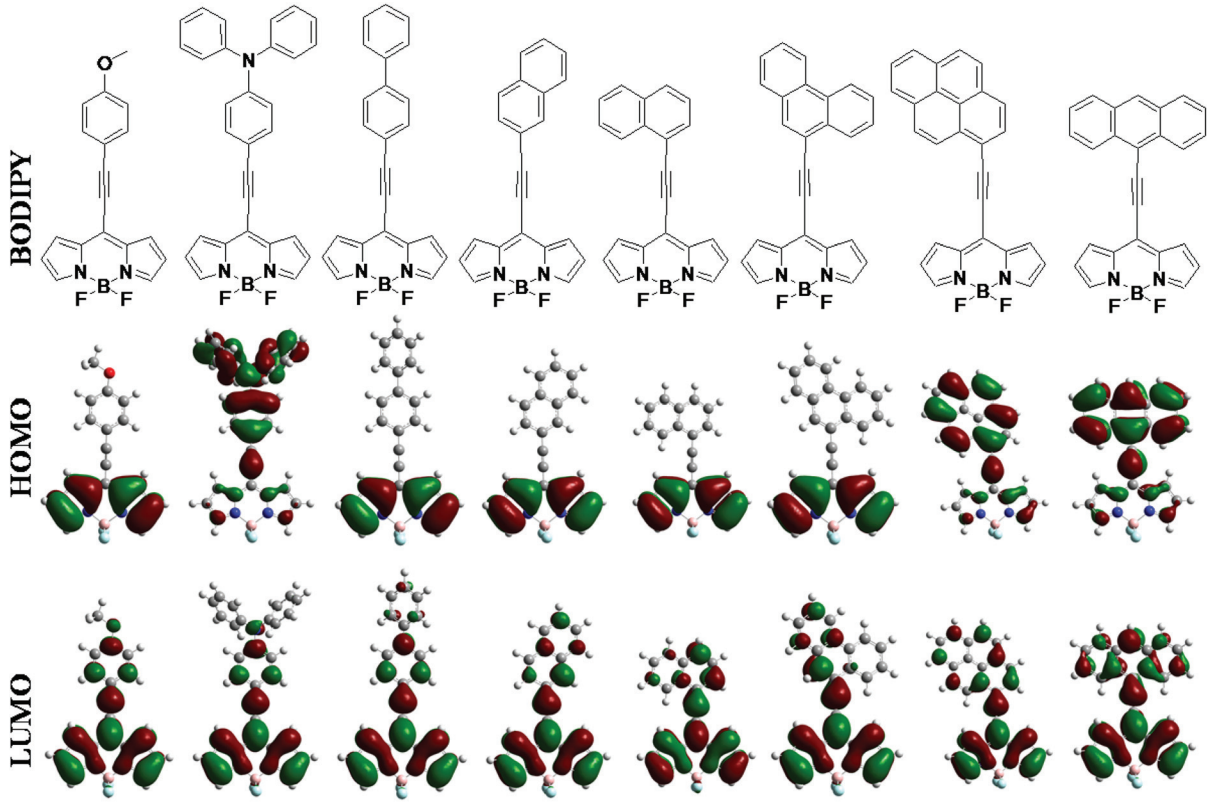


Fig. 6 The HOMO and LUMO frontier molecular orbitals of the *meso*-arylethynyl BODIPYs at the B3LYP/6-31G(d).

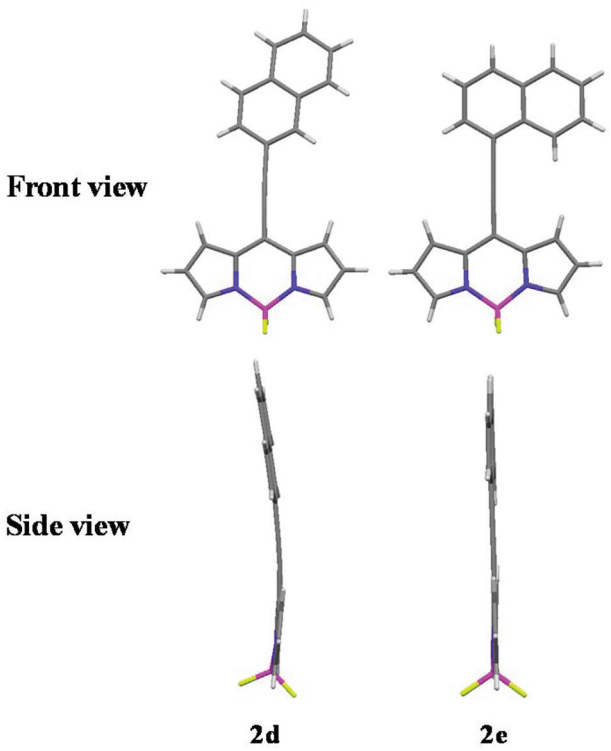


Fig. 7 The single crystals of the BODIPYs **2d** and **2e**, front view and side view.

interesting supramolecular interactions. The NLO properties of these BODIPYs are currently being studied.

## Experimental section

### General methods

The chemicals were used as received unless otherwise indicated. All oxygen or moisture sensitive reactions were performed under a nitrogen/argon atmosphere using the standard Schlenk method. $^{1}$H NMR (400 MHz) and $^{13}$C NMR (100 MHz) spectra were recorded on a 400 MHz NMR instrument using $CDCl_3$ as the solvent. The $^{1}$H NMR chemical shifts are reported in parts per million (ppm) relative to the solvent residual peak ($CDCl_3$, 7.26 ppm). The multiplicities are given as: s (singlet), d (doublet), t (triplet), q (quartet), dd (doublet of doublets), m (multiplet), and the coupling constants, *J*, are given in Hz. The $^{13}$C NMR chemical shifts are reported relative to the solvent residual peak ($CDCl_3$, 77.36 ppm). The thermogravimetric analyses were performed on the Thermal Analysis system at the heating rate of 10 °C per minute under a nitrogen atmosphere. The UV-visible absorption spectra of all of the compounds were recorded on UV-visible Spectrophotometer in dichloromethane. The fluorescence spectra of all the compounds were recorded on a fluorescence spectrophotometer in a dichloromethane solvent. Cyclic voltammograms (CVs) and differential voltammograms (DPVs) were recorded on an electrochemical analyzer using glassy carbon as the

 

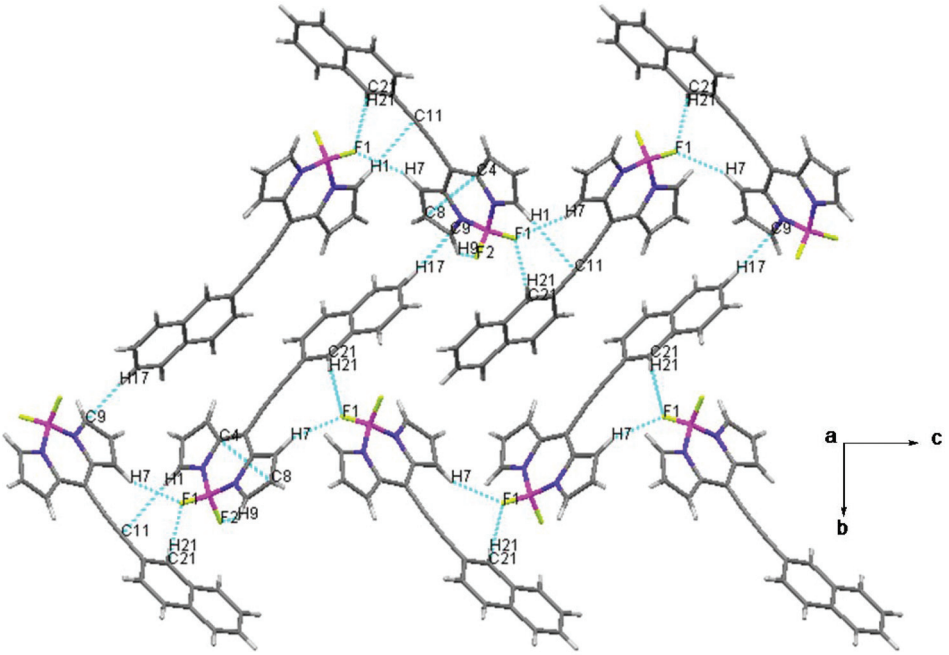


Fig. 8 The crystal packing of **2d**.

working electrode, Pt wire as the counter electrode, and Saturated Calomel Electrode (SCE) as the reference electrode. HRMS was recorded on a mass spectrometer (ESI-TOF).

## Synthesis and characterization

**A generalized procedure for the Sonogashira coupling reaction.** 8-Chloro BODIPY **1** (190 mg, 0.845 mmol) and the corresponding arylethyne (0.845 mmol) were dissolved in THF–triethylamine (10 : 1, v/v; 5 ml), and the mixture was cooled to 0 °C using an ice bath. The reaction mixture was purged with argon, and $Pd(PPh_3)_2Cl_2$ (29.6 mg, 5 mol%), and CuI (16 mg, 10 mol%) were added, followed by stirring at 0 °C for 30 min. Upon the completion of the reaction, the mixture was evaporated to dryness, and the crude product was dissolved in $CH_2Cl_2$, chromatographed on silica (1 : 1; hexanes–$CHCl_3$), and recrystallized from a chloroform–hexane (1 : 3) mixture to give **2a–2h** (yield 44–77%) as purple crystalline solids.

**2a**

Yellow-red crystalline solid. Yield: 77% (110 mg).

$^1$H NMR ($CDCl_3$, 400 MHz, ppm): $\delta$ 7.81 (s, 2H), 7.61 (d, $J$ = 8 Hz, 2H), 7.38 (d, $J$ = 4 Hz, 2H), 6.96 (d, $J$ = 8 Hz, 2H), 6.34 (d, $J$ = 4 Hz, 2H) 3.88 (s, 3H).

$^{13}$C NMR ($CDCl_3$, 100 MHz, ppm): 162.2, 143.1, 136.5, 135.0, 128.9, 128.3, 118.2, 114.8, 113.0, 107.7, 84.4, 55.7.

HRMS (ESI-TOF) $m/z$ = calculated for $C_{18}H_{13}BF_2N_2O$ + $Na^+$ = 345.0984, measured 345.0988.

**2b**

Dark purple crystalline solid. Yield: 44% (90 mg).

$^1$H NMR ($CDCl_3$, 400 MHz, ppm): $\delta$ 7.79 (s, 1H), 7.47 (d, $J$ = 9 Hz, 2H), 7.34 (m, 6H), 7.17 (m, 6H), 7.01 (d, $J$ = 8.8 Hz, 2H) 6.52 (d, $J$ = 3 Hz, 2H).

$^{13}$C NMR ($CDCl_3$, 100 MHz, ppm): 150.8, 146.3, 142.6, 136.3, 134.5, 129.9, 128.4, 126.2, 125.1, 120.5, 118.00, 112.1, 109.3, 85.6.

HRMS (ESI-TOF) $m/z$ = calculated for $C_{29}H_{20}BF_2N_3$ + $Na^+$ = 482.1616, measured 482.1615.

**2c**

Red crystalline solid. Yield: 64% (105 mg).

$^1$H NMR ($CDCl_3$, 400 MHz, ppm): $\delta$ 7.84 (s, 2H), 7.74 (d, $J$ = 8 Hz, 2H), 7.69 (d, $J$ = 8 Hz, 2H) 7.65 (m, 2H), 7.49 (m, 2H), 7.42 (m, 3H), 6.56 (d, $J$ = 4 Hz, 2H).

$^{13}$C NMR ($CDCl_3$, 100 MHz, ppm): 144.0, 143.7, 139.8, 136.7, 133.4, 129.2, 128.5, 127.6, 127.5, 127.27, 119.7, 118.5, 106.1, 85.1.

HRMS (ESI-TOF) $m/z$ = $[M + Na]^+$ calculated for $C_{23}H_{15}BF_2N_2$ + $Na^+$ = 391.1193, measured 391.1197.

**2d**

Red crystalline solid. Yield: 73% (110 mg).

$^1$H NMR ($CDCl_3$, 400 MHz, ppm): $\delta$ 8.23 (s, 2H), 7.88 (m, 5H), 7.65 (dd, $J$ = 1.50 Hz and $J$ = 8.54 Hz, 1H), 7.59 (m, 2H), 7.47 (d, $J$ = 4 Hz, 4H), 6.58 (d, $J$ = 4 Hz, 2H).

$^{13}$C NMR ($CDCl_3$, 100 MHz, ppm): 143.8, 136.7, 134.2, 134.1, 132.9, 129.2, 128.9, 128.4, 128.2, 128.1, 127.6, 127.4, 118.5, 118.2, 106.6, 84.7.

HRMS (ESI-TOF) $m/z$ = calculated for $C_{21}H_{13}BF_2N_2$ + $Na^+$ = 365.1036, measured 365.1039.

**2e**

Red crystalline solid. Yield: 65% (99 mg).

$^1$H NMR ($CDCl_3$, 400 MHz, ppm): $\delta$ 8.35 (dd, $J$ = 8 Hz, 1H), 7.02 (d, $J$ = 8 Hz, 1H), 7.94 (m, 2H), 7.87 (s, 2H), 7.71 (m, 1H) 7.62 (m, 1H), 7.56 (dd, $J$ = 8 Hz, 1H), 7.51 (d, $J$ = 4 Hz, 2H).

$^{13}$C NMR ($CDCl_3$, 100 MHz, ppm): 143.8, 136.7, 133.4, 133.3, 133.2, 132.0, 129.2, 129.0, 128.1, 127.5, 127.2, 125.6, 125.5, 118.64, 118.60, 104.4, 89.0.

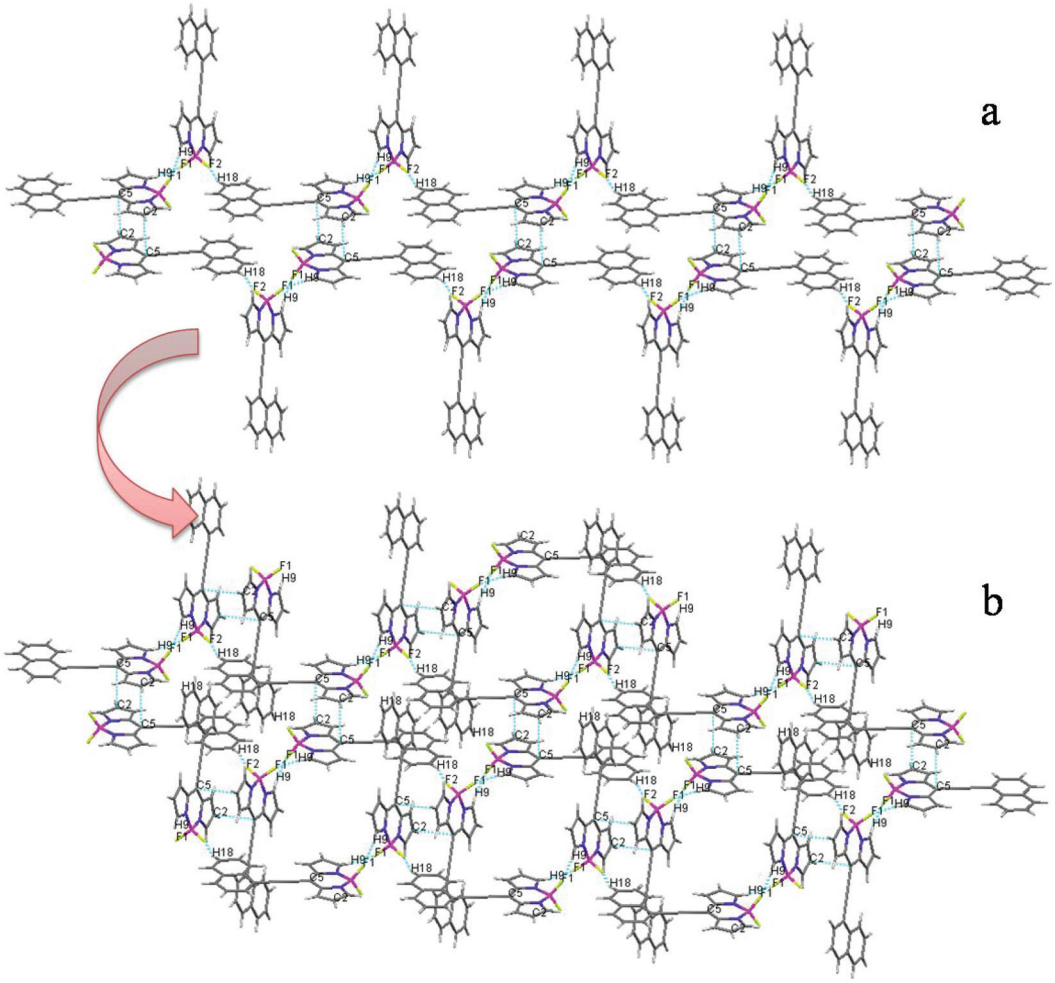


Fig. 9 The crystal packing of **2e** along the tilted *c*-axis.

HRMS (ESI-TOF) *m*/*z* = calculated for $C_{21}H_{13}BF_2N_2$ + $Na^+$ = 365.1036, measured 365.1036.

**2f**

Red crystalline solid. Yield: 57% (99 mg).

$^1$H NMR ($CDCl_3$, 400 MHz, ppm): $\delta$ 8.73 (m, 1H), 8.69 (d, $J$ = 8 Hz, 1H), 8.40 (m, 1H), 8.24 (s, 1H), 7.93 (d, $J$ = 8 Hz, 1H), 7.88 (s, 2H), 7.77 (m, 3H), 7.67 (m, 1H), 7.52 (d, $J$ = 2 Hz, 2H), 6.60 (d, $J$ = 4 Hz, 2H).

$^{13}$C NMR ($CDCl_3$, 100 MHz, ppm): 143.8, 136.8, 135.7, 131.6, 130.8, 130.6, 130.3, 129.4, 129.3, 127.9, 127.9, 127.6, 127.4, 126.5, 123.4, 123.0, 118.6, 117.6, 104.7, 88.6.

HRMS (ESI-TOF) *m*/*z* = calculated for $C_{25}H_{15}BF_2N_2$ + $Na^+$ = 515.1193, measured 5151.1190.

**2g**

Dark purple crystalline solid. Yield: 47% (87 mg).

$^1$H NMR ($CDCl_3$, 400 MHz, ppm): $\delta$ 8.52 (d, $J$ = 8 Hz, 2H), 8.22 (m, 6H), 8.08 (m, 2H), 7.88 (s, 2H), 7.54 (d, $J$ = 4 Hz, 2H), 6.61 (d, $J$ = 8 Hz, 2H).

$^{13}$C NMR ($CDCl_3$, 100 MHz, ppm): 143.4, 136.6, 133.6, 133.5, 131.2, 131.1, 130.9, 130.1, 130.0, 128.9, 127.7, 127.3, 127.0, 126.9, 124.9, 124.8, 124.5, 124.1, 118.5, 114.9, 106.3.

HRMS (ESI-TOF) *m*/*z* = calculated for $C_{27}H_{15}BF_2N_2$ + $Na^+$ = 439.1193, measured 439.1194.

**2h**

Dark purple crystalline solid. Yield: 62% (108 mg).

$^1$H NMR ($CDCl_3$, 400 MHz, ppm): $\delta$ 8.62 (s, 1H), 8.56 (m, 2H), 8.09 (d, $J$ = 8 Hz, 2H), 7.90 (s, 2H), 7.73 (m, 2H), 7.60 (m, 4H), 6.65 (d, $J$ = 4 Hz, 2H).

$^{13}$C NMR ($CDCl_3$, 100 MHz, ppm): 143.4, 136.5, 134.1, 132.0, 131.2, 129.5, 129.0, 128.5, 127.5, 126.3, 126.0, 118.6, 114.5, 103.8, 95.9.

HRMS (ESI-TOF) *m*/*z* = calculated for $C_{25}H_{15}BF_2N_2$ + $Na^+$ = 415.1193, measured 415.1198.

## Acknowledgements

RM thanks CSIR and DST, New Delhi for financial support. BD and TJ thank CSIR and UGC, New Delhi for their fellowship. We are thankful to Sophisticated Instrumentation Centre (SIC), Single Crystal X-ray diffraction Facility, IIT Indore.

 

## References

1 (*a*) A. B. Nepomnyashchii and A. J. Bard, *Acc. Chem. Res.*, 2012, **45**, 1844–1853; (*b*) O. A. Bozdemir, R. Guliyev, O. Buyukcakir, S. Selcuk, S. Kolemen, G. Gulseren, T. Nalbantoglu, H. Boyaci and E. U. Akkaya, *J. Am. Chem. Soc.*, 2010, **132**, 8029; (*c*) N. Boens, V. Leen and W. Dehaen, *Chem. Soc. Rev.*, 2012, **41**, 1130–1172.

2 (*a*) J. Chen, M. Mizumura, H. Shinokubo and A. Osuka, *Chem.–Eur. J.*, 2009, **15**, 5942–5949; (*b*) E. Y. Schmidt, B. A. Trofimov, A. I. Mikhaleva, N. V. Zorina, N. I. Protzuk, K. B. Petrushenko, I. A. Ushakov, M. Y. Dvorko, R. Mealllet-Renault, G. Clavier, T. T. Vu, H. T. T. Tran and R. B. Pansu, *Chem.–Eur. J.*, 2009, **15**, 5823–5830; (*c*) G. Ulrich, R. Ziessel and A. Harriman, *Angew. Chem., Int. Ed.*, 2008, **47**, 1184–1201; (*d*) X. Yin, Y. Li, Y. Zhu, X. Jing, Y. Li and D. Zhu, *Dalton Trans.*, 2010, **39**, 9929–9935.

3 (*a*) M. Baruah, W. Qin, R. A. L. Vallee, D. Beljonne, T. Rohand, W. Dehaen and N. Boens, *Org. Lett.*, 2005, **7**, 4377; (*b*) T. Rohand, M. Baruah, W. Qin, N. Boens and W. Dehaen, *Chem. Commun.*, 2006, 266; (*c*) T. Rohand, W. Qin, N. Boens and W. Dehaen, *Eur. J. Org. Chem.*, 2006, 4658; (*d*) V. Leen, T. Leemans, N. Boens and W. Dehaen, *Chem. Commun.*, 2009, 4515; (*e*) V. Leen, E. Braeken, K. Luckermans, C. Jackers, M. Van der Auweraer, N. Boens and W. Dehaen, *Eur. J. Org. Chem.*, 2011, 4386; (*f*) L. Li, B. Nguyen and K. Burgess, *Bioorg. Med. Chem. Lett.*, 2008, **18**, 3112; (*g*) J. Han, O. Gonzalez, A. Aguilar-Aguilar, E. Pena-Cabrera and K. Burgess, *Org. Biomol. Chem.*, 2009, **7**, 34.

4 (*a*) P. Gautam, B. Dhokale, V. Shukla, C. P. Singh, K. S. Bindra and R. Misra, *J. Photochem. Photobiol., A*, 2012, **239**, 24–27; (*b*) B. Dhokale, P. Gautam and R. Misra, *Tetrahedron Lett.*, 2012, **53**, 2352–2354; (*c*) P. Gautam, B. Dhokale, S. M. Mobin and R. Misra, *RSC Adv.*, 2012, **2**, 12105–12107; (*d*) R. Maragani, T. Jadhav, S. M. Mobin and R. Misra, *Tetrahedron*, 2012, **68**, 7302–7308; (*e*) B. Dhokale, P. Gautam, S. M. Mobin and R. Misra, *Dalton Trans.*, 2013, **42**, 1512–1518; (*f*) R. Maragani, T. Jadhav, S. M. Mobin and R. Misra, *RSC Adv.*, 2013, **3**, 2889–2892; (*g*) R. Misra, P. Gautam, R. Sharma and S. M. Mobin, *Tetrahedron Lett.*, 2013, **54**, 381–383; (*h*) T. Jadhav, R. Maragani, R. Misra, V. Sreeramulu, D. N. Rao and S. M. Mobin, *Dalton Trans.*, 2013, **42**, 4340–4342; (*i*) R. Sharma, P. Gautam, S. M. Mobin and R. Misra, *Dalton Trans.*, 2013, **42**, 5539; (*j*) R. Misra, P. Gautam, T. Jadhav and S. M. Mobin, *J. Org. Chem.*, 2013, **78**, 4940–4948; (*k*) R. Sharma, R. Maragani, S. M. Mobin and R. Misra, *RSC Adv.*, 2013, **3**, 5785; (*l*) R. Misra, T. Jadhav and S. M. Mobin, *Dalton Trans.*, 2013, **42**, 16614; (*m*) R. Maragani and R. Misra, *Tetrahedron Lett.*, 2013, **54**, 5399–5402.

5 X. Yin, Y. Li, Y. Li, Y. Zhu, X. Tang, H. Zheng and D. Zhu, *Tetrahedron*, 2009, **65**, 8373–8377.

6 (*a*) L. Jiao, W. Pang, J. Zhou, Y. Wei, X. Mu, G. Bai and E. Hao, *J. Org. Chem.*, 2011, **76**, 9988–9996; (*b*) J. Godoy, G. Vives and J. M. Tour, *Org. Lett.*, 2010, **12**, 1464; (*c*) M. J. Ortiz, A. R. Agarrabeitia, G. Duran-Sampedro, J. B. Prieto, T. A. Lopez, W. A. Massad, H. A. Montejano, N. A. Garcia and I. L. Arbeloa, *Tetrahedron*, 2012, **68**, 1153–1162; (*d*) M. Baruah, W. Qin, N. Basaric, W. M. De Borggraeve and N. Boens, *J. Org. Chem.*, 2005, **70**, 4152.

7 V. Leen, P. Yuan, L. Wang, N. Boens and W. Dehaen, *Org. Lett.*, 2012, **14**, 6150.

8 (*a*) K. S. Kusaka, R. Sakamoto, Y. Kitagawa, M. Okumura and H. Nishihara, *Chem.–Asian J.*, 2013, **8**, 723–727; (*b*) K. Graf, T. Korzdorfer, S. Kummel and M. Thelakkat, *New J. Chem.*, 2013, **37**, 1417–1426; (*c*) R. Misra, B. Dhokale, T. Jadhav and S. M. Mobin, *Dalton Trans.*, 2013, **42**, 13658.

9 (*a*) M. J. Plater, S. Aiken and G. Bourhill, *Tetrahedron*, 2002, **58**, 2405–2413; (*b*) D. Kim, K. Yamamoto and K. H. Ahn, *Tetrahedron*, 2012, **68**, 5279–5282.

10 (*a*) Y.-S. Feng, C.-Q. Xie, W.-L. Qiao and H.-J. Xu, *Org. Lett.*, 2013, **15**, 936; (*b*) K. Panthi, R. M. Adhikari and T. H. Kinstle, *J. Phys. Chem. A*, 2010, **114**, 4542–4549; (*c*) S. Hachiya, K. Asai and G. Konishi, *Tetrahedron Lett.*, 2013, **54**, 1839–1841; (*d*) Y. Yang, S. Ji, F. Zhou and J. Zhao, *Biosens. Bioelectron.*, 2009, **24**, 3442–3447; (*e*) A. Nierth, A. Y. Kobitski, G. U. Nienhaus and A. Jaschke, *J. Am. Chem. Soc.*, 2010, **132**, 2646–2654; (*f*) M. Sarobe, L. W. Jenneskens, J. Wesseling, J. D. Snoeijer, J. W. Zwikker and U. E. Wiersum, *Liebigs Ann./Recl.*, 1997, 1207.

11 R. Ziessel, P. Retailleau, K. J. Elliott and A. Harriman, *Chem.–Eur. J.*, 2009, **15**, 10369–10374.

12 P. Yang, J. Zhao, W. Wu, X. Yu and Y. Liu, *J. Org. Chem.*, 2012, **77**, 6166–6178.

13 G. Gritzner and J. Kuta, *Pure Appl. Chem.*, 1984, **56**, 461.